# HIGH-RESOLUTION PIV MEASUREMENTS FOR REAR-END AND HEAD-ON COLLISIONS OF TWO SOLITARY WAVES

Motohiko Umeyama[1], Narumi Ishikawa [1] and Ryota Kobayashi [2]

The flow visualization technique was applied to the collision of two solitary waves propagating in the same and opposite directions. Measurements of the velocity and trajectory of the solitary waves were conducted using a particle image velocimetry (PIV) system consisting of an 8-W ND:YAG laser and a high-speed CCD camera. In the solitary-wave interaction tests, we set up three kinds of velocity fields—smaller, taller, and compound waves in the rear-end collision tests, and right-running, left-running, and colliding waves in the head-on collision tests. Instantaneous and spatial surface profiles were measured using the image thresholding method in which the boundary plane between the air and water can be detected as the interface having the maximum luminance value. The measured run-up elevation of the colliding wave was compared with the theoretical elevation using a third-order perturbation solution. Based on a Eulerian-Lagrangian algorithm, the PIV result was applied to the particle tracking process that occurred in the two-dimensional plane.

*Keywords: Solitary wave; Rear-end Collision; Head-on Collision; PIV; Velocity; Particle trajectory/*

## INTRODUCTION

According to a literature review by Weber and Weber (1825), a few water-wave experiments (Flaugergues 1793 and Coudraye 1796) were conducted before 1800. In the early nineteenth century, however, linear and nonlinear wave theories progressed quickly in France and Germany, respectively. Poisson (1818) and Cauchy (1827) conducted research on 2D linear sinusoidal waves in a finite depth, while Gerstner (1802) studied rotational waves in deep water. British scientists of that time made few original contributions to the subject of wave theories, because they did not even know linear wave theory well. In 1837, the British Association for the Advancement of Science set up a "Committee on Waves" with John Scott Russell and Sir John Robison as the sole members. This committee conducted surface wave experiments using a long wave tank, and published a substantial report (1837) in which they distinguished four types of waves: solitary, oscillatory, capillary, and corpuscular waves. After their laboratory study, the mechanism of surface waves in canals was investigated by several mathematicians, including Green (1838), who was the first to attempt to model Russell-Robison's long wave observations in variable vertical shapes, and Kelland (1840), who described solitary-wave motion in arbitrary depths. In contrast, Airy (1841) described the Weber-Weber literature review and the Russell-Robinson experiments in his article "Tides and Waves," but he couldn't convince himself of their "The Great Primary Wave" experimental result or the solitary wave, because the observed wave contradicted his own linear shallow-water wave theory. The issue at that time was the problem of permanent profile waves. The formula for celerity of Airy's harmonic wave disagreed substantially with that of their solitary wave. Airy's celerity formula was independent of the height of the disturbance above the still water level but showed a noticeable dependence on wave height or a typical nonlinear feature. Russell expressed disappointment in Airy's remarks about the contents of the 1837 report and objected to his opinion in his "Report on Waves" (1844). Russell's prediction was finally independently confirmed by both Boussinesq (1871) and Rayleigh (1876), whereby they derived the celerity of the explicit dependence on the wave height from the equation of motion for an inviscid and incompressible fluid. They also showed that the surface displacement is given by the $\sec h^2$ profile. By considering the balance between nonlinearity and dispersion, Korteweg and de Vries (1895) derived a solution for a solitary wave propagating alone, in which the KdV theory of a first-order approximation can adequately explain the solitary-wave's properties, and the theoretical wave profile agreed well with the surface displacement observed by Russell. The solitary wave was considered a relatively unimportant curiosity in the field of nonlinear waves for some time after the work of Korteweg and de Vries. Since the 1950s, however, the KdV equation and other equations, which admit solitary-wave solutions, have been the subject of intense study. Scientists remain intrigued by the physical properties and elegant mathematical theories of the shallow-water wave. A formula describing the surface displacement of a single solitary wave was solved to the second-order by Laitone (1960), to the ninth-order by Fenton (1972), and to the

[1] Department of Civil & Environmental Engineering, Tokyo Metropolitan University, 1-1 Minami-ohsawa, Hachioji, Tokyo 192-0397, Japan
[2] Tokyo Metropolitan Government, 2-8-1 Nishi-Shinjuku, Shinjuku-ku, Tokyo 163-8001, Japan

70th-order by Schwartz (1974).

Russell's report (1844) motivated Stokes to work toward an irrotational oscillatory wave with open water-particle orbits; i.e., a Stokes wave whose amplitude is not necessarily small. Stokes (1847) developed the second-order theory for finite amplitude waves using a power series based on the ratio of the amplitude to wavelength known as the Stokes expansion, which is viewed as one of the modern method cornerstones in the study of weakly nonlinear wave theory. There is no doubt that Russell's work is one of the greatest early contributions to mechanisms not only for solitary wave but also for the oscillatory wave. Needless to say, his measurement was unique and astonishingly accurate in the period before the innovation of electric equipment.

Just after the mid-twentieth century, a surprising or unusual fact was revealed regarding the KdV equation (Fermi et al. 1955). Zabusky and Kruskal (1965) found from numerical solutions of the KdV equation that multiple solitary waves retain their original shapes and speeds, but they undergo a phase shift with respect to each other after a rear-end collision. The exact solution of the KdV equation for collisions of multiple solitary waves was first given by Hirota (1971). Byatt-Smith (1971) obtained some approximate analytical solutions, including a second-order approximation, for the reflection of a solitary wave by a vertical wall. The Boussinesq equation admitted solutions that consisted of two solitary waves (incident and reflected waves), with each solitary wave satisfying an appropriate KdV equation. A smaller-order interaction term has been added to separate the two solitary-wave terms into functions of their respective phase variables.

Head-on collision experiments were performed by Chan and Street (1970), and Maxworthy (1976). The significant results of these experiments were the phase shift whose magnitude was independent of the wave amplitude, and the maximum run-up height that was greater than twice the initial wave amplitude during reflection at a vertical wall. The major quantitative difference between the theory of Byatt-Smith (1971) and the experiment of Maxworthy (1976) was in the magnitude of the spatial phase shift, where the theory gave a square root dependence on wave amplitude. The experiment of Renouard et al. (1985) also showed that there was a transient loss of amplitude in the reflected wave but this loss was recovered after sufficient time had elapsed. This observation could be explained by the presence of the dispersive tail behind the solitary wave. On the other hand, Weidman and Maxworthy (1978) performed a series of experiments on the interaction between two shallow-water solitary waves propagating in the same direction in a rectangular channel with the aim of testing Hirota's solution for the interaction of isolated solitary waves. Since then, experimental confirmation of various solitary waves and their interactions has been provided in many wave tanks (Hammack et al. 2004, Craig et al. 2006), and the findings have led to rapid theoretical development (Fenton and Rienecker 1982, Mirie and Su 1982, Byatt-Smith 1987a 1987b, Marchant and Smith 1990). The KdV equation and other equations admitting solitary-wave and soliton solutions have intrigued mathematicians for a half-century (see, e.g., Drazin and Johnson 1989, Remoissenet 1999, Dauxois and Peyrard 2006, and Constantin 2011).

Many investigations have focused on surface properties since the great discovery of the solitary wave, but some researchers have considered the underlying particle velocity and trajectory. In the latter half of the twentieth century, experimental studies have generally relied on point measurement techniques. Modern electric equipment is excellent for measuring fluid velocities, but it has other limitations. Recently, visualization techniques have played a more important role, yielding both qualitative and quantitative insights in wave kinematics. Significant developments in particle image velocimetry (PIV) and particle tracking velocimetry (PTV) have enabled the visualization of velocity fields and particle paths. The PIV technique evaluates instantaneous velocities by recording the position of images of small tracers that are suspended in the fluid at successive instants in time. In contrast, PTV measures the velocity of each particle in a 2D slice, with respect to its frames and separated by a time interval, and then reconstructs the flow field from the velocity at the seeding particle location points. We have investigated internal waves propagating in a two-layer system using PIV. Shimizu et al. (2006), Umeyama (2008), Umeyama and Shinomiya (2009), Umeyama and Matsuki (2011), Umeyama and Nguyen (2012), and Umeyama et al. (2012) set up an apparatus to measure the instantaneous velocity of internal waves with an illumination source (frequency-doubled Nd:YAG laser with 50 mW of energy at 532 nm) and a camera (CCD or high-definition digital video camera). Using the same PIV system, Umeyama et al. (2010) and Umeyama (2011, 2012) measured and analyzed the water particle velocity and trajectory for surface Stokes waves with and without a steady current. In this study, we focus on the collision of two solitary waves using a new PIV system, which improves the spatial resolution of the previous PIV analysis. Following a precedent set by Umeyama (2013), we estimate the velocity vector

and trajectory of each particle. Measurements of the water surface are also made using the image thresholding method.

## THEORIES

A solitary wave propagates in a 2D channel in which the motion is identical in any direction parallel to the crest line. Consider a cross section of the wave field that is perpendicular to the crest line with Cartesian coordinates $(x, z)$, with the $x$-axis being the direction of the wave propagation and the $z$-axis pointing vertically upward, and with the origin laying on the flat bottom. Dean and Dalrymple (1984) gave the surface elevation as

$$\eta = a \sec h^2 \sqrt{\frac{3}{4}\frac{a}{h^3}} x \tag{1}$$

where $a$ = wave amplitude, and $h$ =depth. The celerity was defined as

$$c = \sqrt{gh}(1 + \frac{a}{2h}) \tag{2}$$

where $g$ = gravity acceleration.

We also determined the velocity of a water particle under a solitary wave. The horizontal and vertical velocity components became

$$u = c\left(-1 + \left(\frac{a}{h} + 3\left(\frac{a}{h}\right)^2\left(\frac{1}{6} - \frac{1}{2}\left(\frac{z}{h}\right)^2\right)\right)\frac{\eta}{a} - \left(\frac{a}{h}\right)^2\left(\frac{7}{4} - \frac{9}{4}\left(\frac{z}{h}\right)^2\right)\left(\frac{\eta}{a}\right)^2\right) \tag{3}$$

$$w = c\sqrt{\frac{3a}{h}}\frac{z}{h}\frac{\eta}{h}\tanh\sqrt{\frac{3a}{4h^3}}x\left(1 + \frac{a}{2h}\left(1 - 7\frac{\eta}{a} - \left(\frac{z}{h}\right)^2\left(1 - \frac{3\eta}{a}\right)\right)\right) \tag{4}$$

For a head-on collision of two solitary waves, Su and Mirie (1980) derived a third-order solitary-wave solution using the perturbation method. They expressed the surface elevation as

$$\begin{aligned}\eta(x,t) = {} & \varepsilon_R\left(\eta_R + \frac{3}{4}\varepsilon_R\left(\eta_R^2 - \eta_R\right) + \varepsilon_R^2\left(\frac{101}{80}\eta_R^3 - \frac{151}{80}\eta_R^2 + \frac{5}{8}\eta_R\right)\right) \\ & + \varepsilon_L\left(\eta_L + \frac{3}{4}\varepsilon_L\left(\eta_L^2 - \eta_L\right) + \varepsilon_L^2\left(\frac{101}{80}\eta_L^3 - \frac{151}{80}\eta_L^2 + \frac{5}{8}\eta_L\right)\right) \\ & + \varepsilon_R\varepsilon_L\left(\frac{1}{2} + \left(\frac{7}{4}\left(\varepsilon_R\eta_R + \varepsilon_L\eta_L\right) - \frac{11}{8}\left(\varepsilon_R + \varepsilon_L\right)\right)\right)\eta_R\eta_L\end{aligned} \tag{5}$$

with $$\eta_R = a_R \sec h^2\left(h\left(\frac{3\varepsilon_R}{4}\right)^{\frac{1}{2}}\left(1 - \frac{5}{8}\varepsilon_R + \frac{71}{128}\varepsilon_R^2\right)\left(x - c_R t + \theta\right)\right) \tag{6}$$

and $$\eta_L = a_L \sec h^2\left(h\left(\frac{3\varepsilon_L}{4}\right)^{\frac{1}{2}}\left(1 - \frac{5}{8}\varepsilon_L + \frac{71}{128}\varepsilon_L^2\right)\left(x + c_L t + \theta\right)\right) \tag{7}$$

where $\varepsilon_R = a_R / h$, $\varepsilon_L = a_L / h$, $a_R$ = right-running-wave amplitude, $a_L$ = left-running-wave amplitude, $c_R$ =right-running-wave celerity, $c_L$ =left-running-wave celerity, and $\theta$ =phase.

## EXPERIMENTS AND ANALYSES

We performed experiments in a wave tank 25.0 m long, 0.8 m wide, and 1.0 m deep (see Figure 1). The wave tank consisted of 10 steel flanges and 12 glass panels 90 cm long, 73 cm high, and 1.0 cm thick. The wave-generating system consisted of a servo controlling device and a vertical plate that moved horizontally at one end of the tank. For the single solitary wave and rear-end collision experiments, a wave absorber was installed at the other end of the tank. The wave absorber consisted of a vinylidene chloride mat that limited the reflection to 5% over a wide range of test conditions. For the head-on collision experiments, a vertical wall was fabricated at the end of the tank. The wave-generating system accepted a programmed input electrical signal into a displacement that was directly proportional to the magnitude of the voltage. Hence, the displacement-time history, or the wave paddle trajectory, of the movement was proportional to the voltage-time history of the input signal. We used a 14-bit arbitrary waveform generator (Wave Station 2022, Teledyne LeCroy) to control the movement of the wave paddle and to create highly accurate and repeatable solitary waves. A variety of modulation

schemes, intuitive waveform editing software, and remote control capabilities enabled the versatile generation of waveforms up to 160 MHz. The maximum sample rate was 125 MS/s and the memory contains about 16,000 points. This arbitrary waveform generator allowed almost unlimited programming flexibility for the wave paddle motion, and although it had some mechanical limitations, the wave generating system was still flexible in its operation. The exact position of the wave paddle was determined by the servo controlling device. The test section was located in an area between 14.0 m and 15.0 m downstream of the wave paddle.

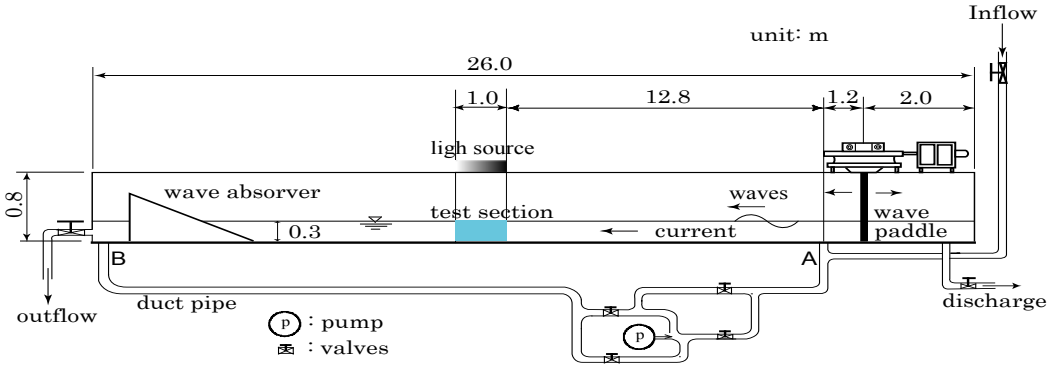


**Figure 1. Sketch of apparatus.**

Based on the extensive experimental data supporting wave generation theory, Goring (1979) proposed the following formula for generating a solitary wave,

$$\xi(t) = A\tanh 7.6\left(\frac{t}{\tau}-\frac{1}{2}\right) \text{ where } A = 4\sqrt{\frac{ah}{3}} \text{ , and } \tau = \frac{4}{\sqrt{g(h+a)}}\sqrt{\frac{h^3}{3a}}\left(\tanh^{-1}(0.999)+\frac{a}{h}\right)$$

where $A$ =stroke and $\tau$ =duration of motion. The oscillatory tail, which is approximately 25% of the height of the main wave when a linear trajectory is being used, could be reduced to approximately 10%.

Therefore, in our experiment, we have used Goring's theory for generating single and dual solitary waves. The trajectory of the wave paddle for a single solitary wave is given by,

$$\xi(t) = \begin{cases} \dfrac{A}{2}\tanh\left(2\pi\left(\dfrac{t}{\tau}-\dfrac{1}{2}\right)\right)+\dfrac{A}{2}\tanh\pi & 0 \le t \le \tau \\ A\tanh\pi & t \ge \tau \end{cases}$$

Figure 2 shows an example of the wave paddle motion and the programmed signal for $A$ =100 mm and $\tau$ =1.2 s.

The arbitrary waveform generator can prescribe the motion that creates the dual solitary waves. Figure 3 shows the programmed input signal to control the wave paddle motion. There are seven duration periods: (i) the wave paddle moves toward the initial position (150 mm from the center); (ii) a stationary period (50 s); (iii) the first wave is generated; (iv) a stationary period; (v) the second wave is generated; (vi) a stationary period; and (vii) the wave paddle moves toward the initial position. In the case of two solitary waves traveling in the same direction, the second wave is generated immediately after the first wave moves toward the far end of the tank so that the second wave passes the first wave at a fixed location in the tank. In the case of counter-propagating solitary waves, while the first wave is reflected from the vertical wall set at the end and propagates backward toward the wavemaker, the second wave is generated so that these two waves collide head-on near the center of the test section.

The image thresholding method has been used to study the spatial variations of a water surface. This method was originally designed to reduce a grayscale image to a binary image (Umeyama 2008). The algorithm assumes that the image contains two classes of pixels following a bi-modal histogram (object and background pixels). It calculates the optimum threshold separating the two classes. In the present study, a laser sheet induces the water to fluoresce and identifies a water-surface profile as the threshold's spatial distribution. The processed data were saved to ASCII files and transformed to real scale during the analysis.

For velocity measurement, we employed PIV based on a single-exposure image. The instantaneous water particle velocity was observed using a PIV system consisting of an 8-W frequency-doubled Nd:YAG laser (LaVision Flow Master) and a high-speed CCD camera (Photoron's FASTCAM SA4).

The laser consists of a laser head (FKLA-800e), power supply (LABP-D40-CW), and a visualization probe (LVS) connected to the laser head with an optical fiber. The probe was set at a beam and fabricated above the wave tank (approximately 120 cm from the bottom), and then emitted a laser sheet 2 mm thick from an upper point toward the water surface. This light sheet had very uniform intensity and was well suited to PIV measurement over a large area. The frame rate of the CCD camera was 3,600 fps for a maximum resolution of 1,024×1,024 pixels, although this new technology can follow a fast particle motion at 500,000 fps at a resolution of 128×16 pixels. The CCD camera was arranged in a line 2 m from the sidewall of the wave tank to cover an area up to 60.0 cm×20.0 cm. The water in the tank was seeded with DIAION (DK-FINE HP20), having a grain size of 0.25 mm and a specific gravity of 1.01. Vector fields were obtained with the PIV system by processing a pair of image frames of 1024×800 pixels at 250 fps. The size of the interrogation window was set to 8×8 pixels and the size of the candidate region was set to 16×16 pixels.

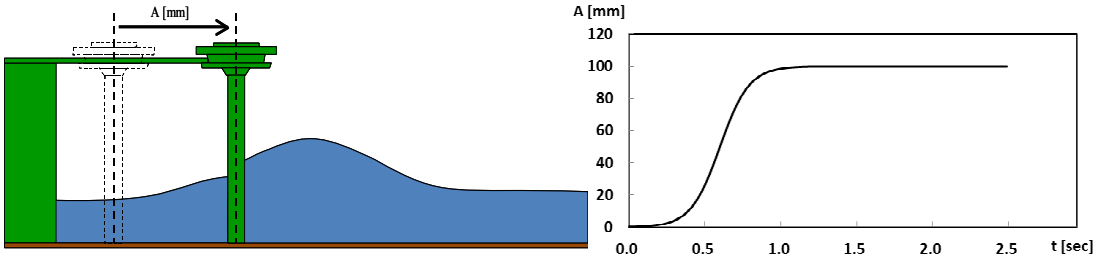


**Figure 2. Wave-paddle motion and programmed signal for a solitary wave.**

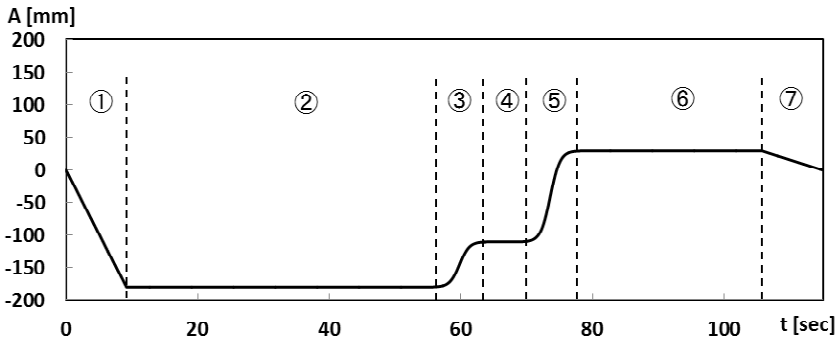


**Figure 3. Programmed signal for two solitary waves.**

**Table 1. Experimental Conditions in the Present Experiment.**

| Case | h (cm) | 1st H (cm) | 2nd H (cm) | Remarks |
|---|---|---|---|---|
| W1 | 5.0 | 1.00 | – | single wave |
| W2 | 5.0 | 1.30 | – | single wave |
| W3 | 5.0 | 2.20 | – | single wave |
| W4 | 10.0 | 1.25 | – | single wave |
| W5 | 10.0 | 2.00 | – | single wave |
| W6 | 10.0 | 3.35 | – | single wave |
| W7 | 15.0 | 1.25 | – | single wave |
| W8 | 15.0 | 2.25 | – | single wave |
| W9 | 15.0 | 4.00 | – | single wave |
| WW1-1 | 5.0 | 1.00 | 2.20 | rear–end collision of W1 and W3 |
| WW1-2 | 10.0 | 1.25 | 3.35 | rear–end collision of W4 and W6 |
| WW1-3 | 15.0 | 1.25 | 4.00 | rear–end collision of W7 and W9 |
| WW2-1 | 5.0 | 1.30 | 1.30 | head–on collision of W2 and W2 |
| WW2-2 | 10.0 | 2.00 | 2.00 | head–on collision of W3 and W3 |
| WW2-3 | 15.0 | 2.25 | 2.25 | head–on collision of W8 and W8 |

In our study, we conducted a series of collision tests for two solitary waves. A summary of the experimental conditions is presented in Table 1. W1–W9 are the single solitary-wave cases. The wave height ranged from 1.0 cm to 4.0 cm, at water depths of 5.0 cm, 10.0 cm, and 15.0 cm. WW1-1, WW1-2, and WW1-3 are the rear-end collision cases. The first and second solitary waves (i.e., W1, W3, W4, W6, W7, and W9) propagate in the same direction and the second wave overtakes the first one in the test section. WW2-1, WW2-2, and WW2-3 are the head-on collision cases by W2, W5, and W8, respectively. The second wave collides with the first one that has been reflected back from the vertical wall set at the end of the wave tank.

## RESULTS

### Rear-end collisions

Figure 4 shows the spatial surface profiles for three rear-end collision cases: (a) WW1-1, (b) WW1-2, and (c) WW1-3. Each panel consists of three wave profiles for the smaller-amplitude, higher-amplitude (taller), and compound waves; for instance, in order of depth, W1 and W3 in WW1-1, W4 and W6 in WW1-2, and W7 and W9 in WW1-3. In all cases, the smaller and taller waves propagate in the right direction. The time at t=0.00 s is the moment when the combined water surface attains maximum elevation, so that the negative and positive signs define the moments before and after the collision, respectively. Figure 4(a) shows the wave profiles at three different times, while the taller wave of $a_{II}$=2.20 cm catches up with and interacts with the shorter wave of $a_{I}$=1.00 cm at a water depth of h=5 cm. We can observe a special type of nonlinear process from the figure. The two waves do not satisfy the linear superposition principle. The combined wave forms a single long wave that gradually increases the water surface elevation before the crest of the taller wave catches up with that of the smaller wave and decreases the surface elevation after the taller wave passes the smaller wave. The surface elevation attains its highest level at this time, which is lower than the taller wave amplitude but higher than the smaller wave amplitude. Very quickly, the taller wave leaves the smaller one behind. The two waves moving in the far positive x region after the collision are identical to the pair that moved in the far negative x region previously, although the dispersion event occurs outside the measurement area. Figure 4(b) presents similar wave profiles for $a_{I}$=1.25 cm, $a_{II}$=3.35 cm, and h=10.0 cm. Both single solitary-wave profiles are symmetrical. The surface of the compound wave rises somewhat before the taller wave overtakes the smaller one, and it decreases gradually before both waves escape unscathed from the rear-end collision. Figure 4(c) shows another example of surface displacements for $a_{I}$=1.25 cm and $a_{II}$=4.00 cm at a deeper depth of h=15.0 cm. In this case, it is clear that the original pattern of each waveform varies entirely during the interaction, and the compound wave behaves like a single wave. The water surface of the compound wave equals that of the taller wave at the left boundary in the measurement area prior to the collision. The former exceeds the latter except at the near-crest region at t=0.00 s. Finally, for a short time after the collision, the surface elevation of the compound wave lies between the taller and smaller wave surfaces.

Figure 5 shows the instantaneous velocity fields for WW1-1 during a rear-end collision. The upper, middle, and lower rows are for the compound, smaller, and taller waves, respectively. These vector maps indicate velocity very precisely while two solitary waves pass in front of the recording area. For both single solitary waves, the measured horizontal velocity is always positive, while the direction of the vertical velocity component is upward before the crest but downward behind it. The horizontal velocity clearly increases from the negative x area to the crest, and thereafter decreases to the positive x area at the same rate. In contrast, the measured vector for the compound wave is almost flat for the total depth during the interaction. The velocities increase gradually with time until t=0.00 s. After that, the wave reduces the water-particle speed until the disappearance of the waves. The experimental result of the compound wave shows a decay in the velocity throughout the area when wave-wave interaction occurs. Generally, the direction of a water particle is the same as that of the wave propagation. It is uncertain from these pictures whether the nonlinear collision effect decreases the velocity. Figure 6 shows the PIV results of the instantaneous velocity maps for WW1-2 together with W4 and W7 at an interval of 0.42 s. A weak velocity appears in front of the smaller and taller waves when the former moves forward for a short distance toward the latter at t=−0.42 s, and the weak velocity appears behind them when the latter is ahead of the former at t=0.42 s. In this case, the interaction reduces the speed of the water particles beneath the crest of the compound wave.

Figure 7 shows the water-particle paths for WW1-2 during a rear-end collision. The circular symbol indicates the instantaneous position of a water particle based on a Eular-Lagrangean algorithm

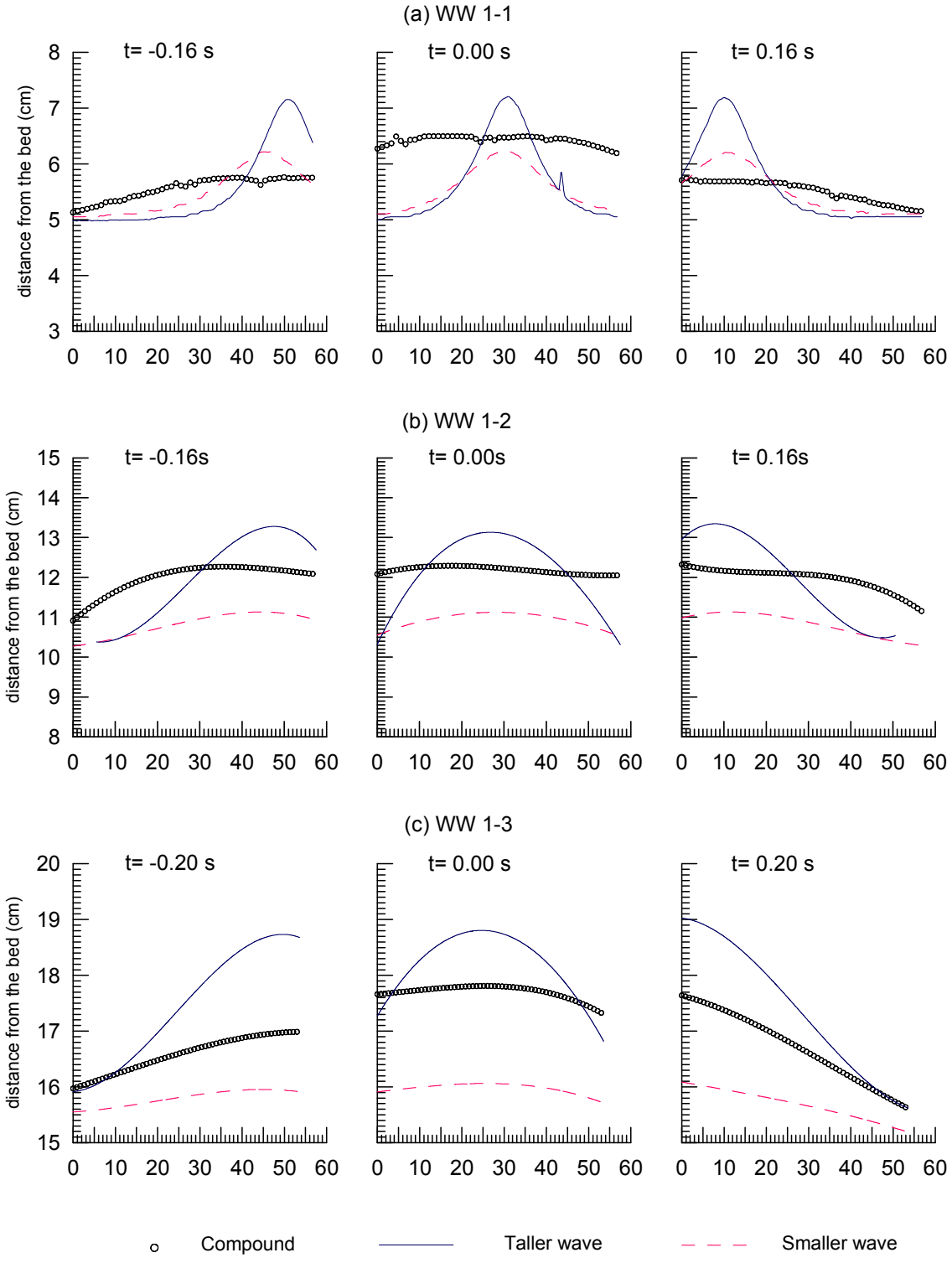


**Figure 4. Water surface displacements for rear-end collisions.**

(Umeyama 2010) using the PIV result. The water-particle paths are plotted at 1 cm intervals between the surface and the bottom. The particle trajectory takes a bell-type path, which flattens toward the bottom. This feature matches with the description of the flow field shown in Figure 6. The distance moved is nearly constant with depth except at the surface where the distance is somewhat shorter.

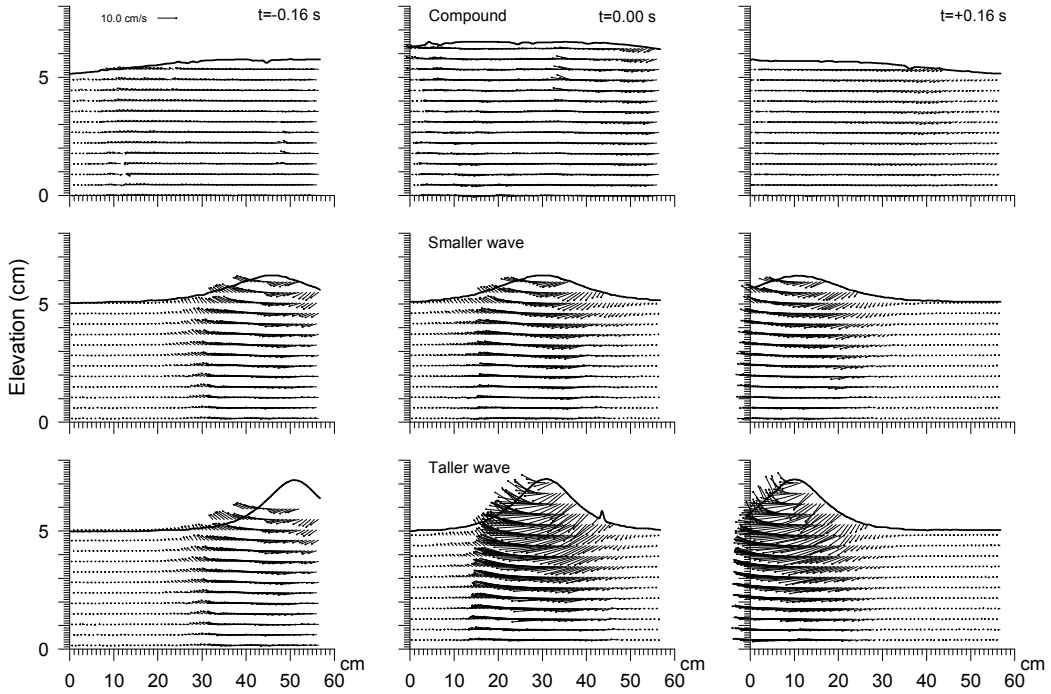


**Figure 5. Experimental results of velocity field for rear-end collision (d=5 cm).**

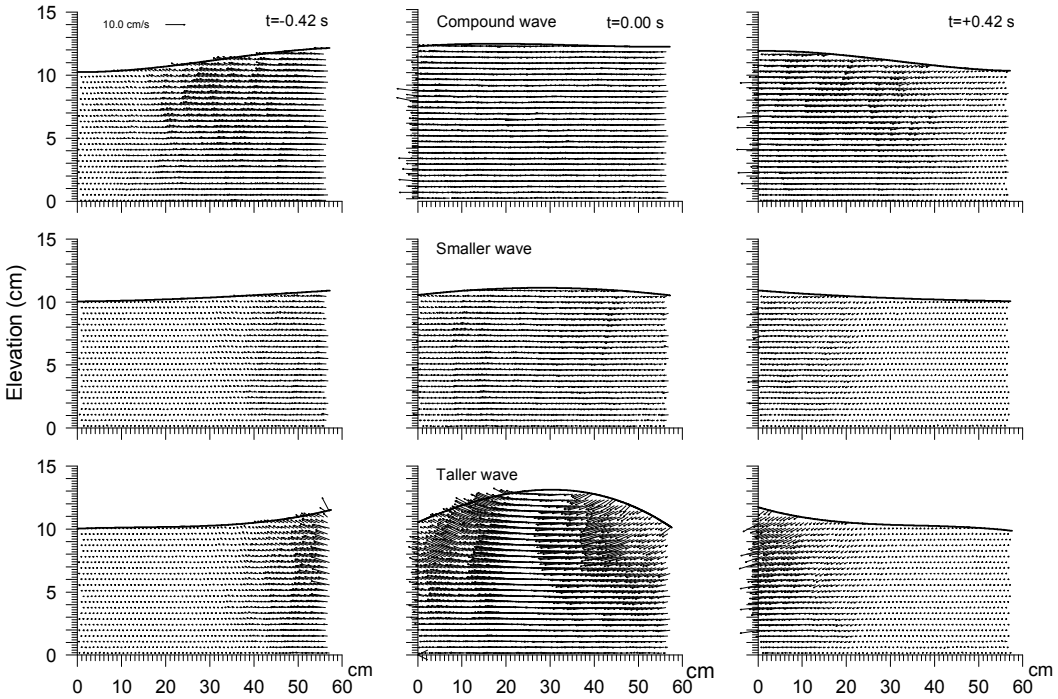


**Figure 6. Experimental results of velocity field for rear-end collision (d=10 cm).**

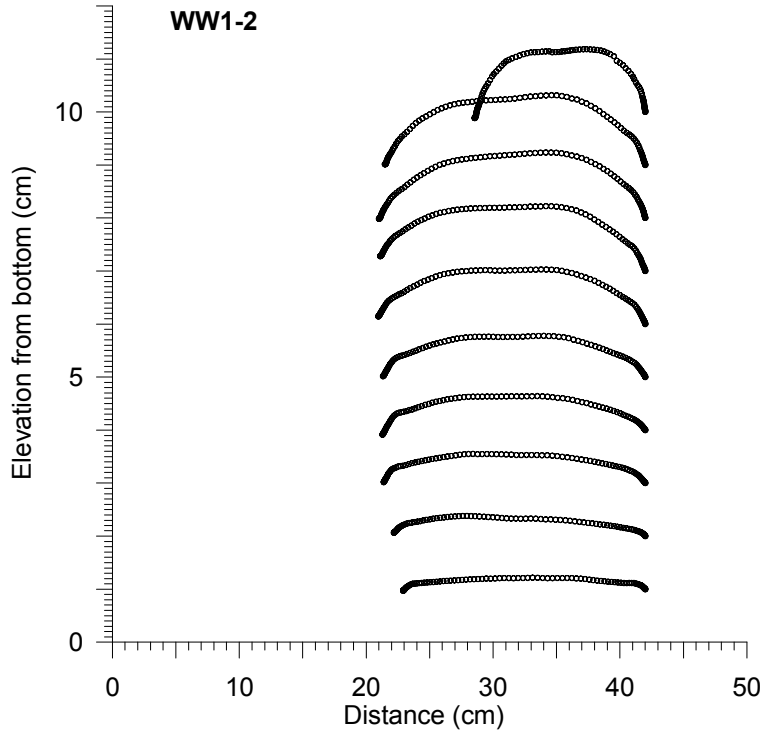


**Figure 7. Particle trajectories for a rear-end collision (d=10 cm).**

**Head-on collisions**

Su and Mirie (1980) calculated the maximum run-up amplitude of a colliding wave formed by two counter-propagating solitary waves. When two solitary waves have identical amplitude, the run-up at the colliding point is defined by the value of the perturbed free surface elevation of Equation (5). The maximum run-up elevation up to $O\{(a/h)^3\}$ exists where $\eta_R = \eta_L = a$, and is expressed as

$$\frac{\eta_{\max}}{h} = 2\frac{a}{h} + \frac{1}{2}\left(\frac{a}{h}\right)^2 + \frac{3}{4}\left(\frac{a}{h}\right)^3 \tag{8}$$

The phase shift of a single solitary wave is

$$\frac{\Delta\theta}{h} = \pm\left(\frac{1}{3}\frac{a}{h}\right)^{\frac{1}{2}}\left(1 + \frac{7}{8}\frac{a}{h}\right) \tag{9}$$

where the + and − signs indicate the right- and left-running waves, respectively.

Figure 8 shows the spatial surface profiles for three head-on collision cases: (a) WW2-1, (b) WW2-2, and (c) WW2-3. The surface profiles were chosen in a similar way to those for the rear-end collision experiments. In each case, the panels were put in the order of the chief moments during the interaction. Two single solitary-wave profiles are superimposed on the measured colliding-wave profile in the panel. The wave moving from left to right (i.e., right-running wave) is coming directly from the wavemaker, while the one moving from right to left (i.e., left-running wave) was reflected from the vertical wall at the end of the tank. Figure 8(a) shows the collision process by two counter-propagating solitary waves of $a_R = a_L$ =1.30 cm for h=5 cm. Two original waves interact with each other and deform between these crests at t=−0.16 s. The water-surface profile of the colliding wave is similar to that of the linear superposition of the right-running and left-running solitary waves. The water surface reaches its maximum level at t=0.00 s. The maximum elevation of the measured water surface is $\eta_{crest}$ =2.77 cm while the theoretical prediction by Su and Mirie (1980) yields $\eta_{\max}$ =2.83 cm. The calculated elevation agrees well with the measured one when the two crests collide. The surface descends to the initial water level at t=0.16 s. The two crests separate from the colliding wave into two solitary waves that shift phase from the original waves. The phase shift calculated using Equation (9) is $\Delta\theta/h = \pm 0.361$. Figure 8(b) shows another colliding wave that emerged by the collision of the right- and left-running solitary waves of amplitude $a = a_R = a_L$ =2.00 cm for h=10 cm. Two waves merge into

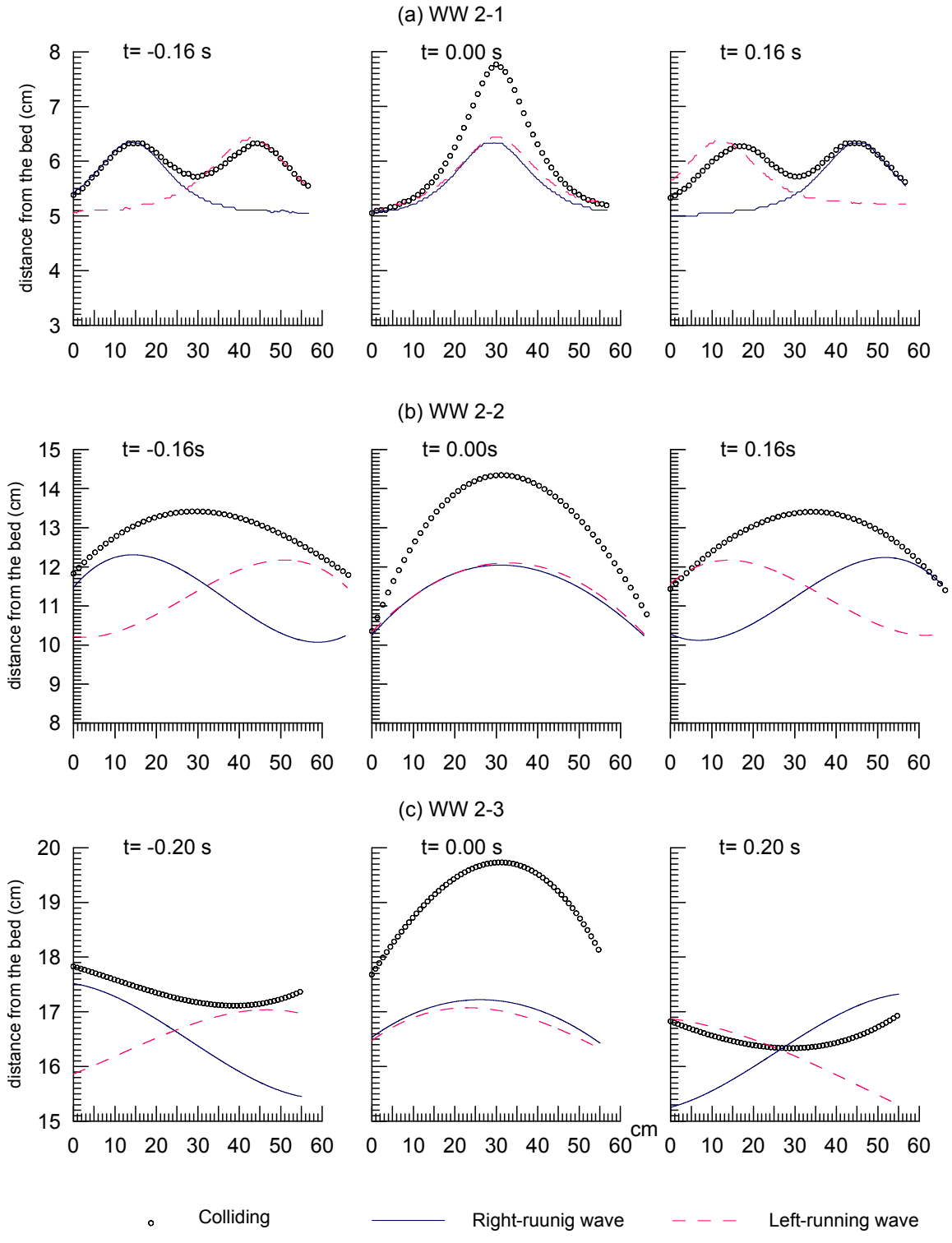


**Figure 8. Water surface displacements for head-on collisions.**

a colliding wave with their interaction at t=−0.16 s, combine completely at t=0.00 s, and maintain their individual wave function at t=0.16 s. The measured and calculated elevation at t=0.00 s is $\eta_{crest}$ =4.35 cm and $\eta_{\max}$ =4.26 cm, respectively, and the phase shift is $\Delta\theta/h = \pm 0.3034$ . Figure 8(c) presents the resulting space-time plots of the surfaces of the two solitary waves and the colliding wave, for $a = a_R = a_L$ =2.25 cm and h=15 cm. In the test, the agreement of the measured surface peak with the theoretical prediction is excellent: $\eta_{crest}$ =4.73 cm and $\eta_{\max}$ =4.71 cm, respectively. The calculated phase shift for the right- and left-running waves is $\Delta\theta/h = \pm 0.253$ , although we cannot make a proper judgment from the figure alone.

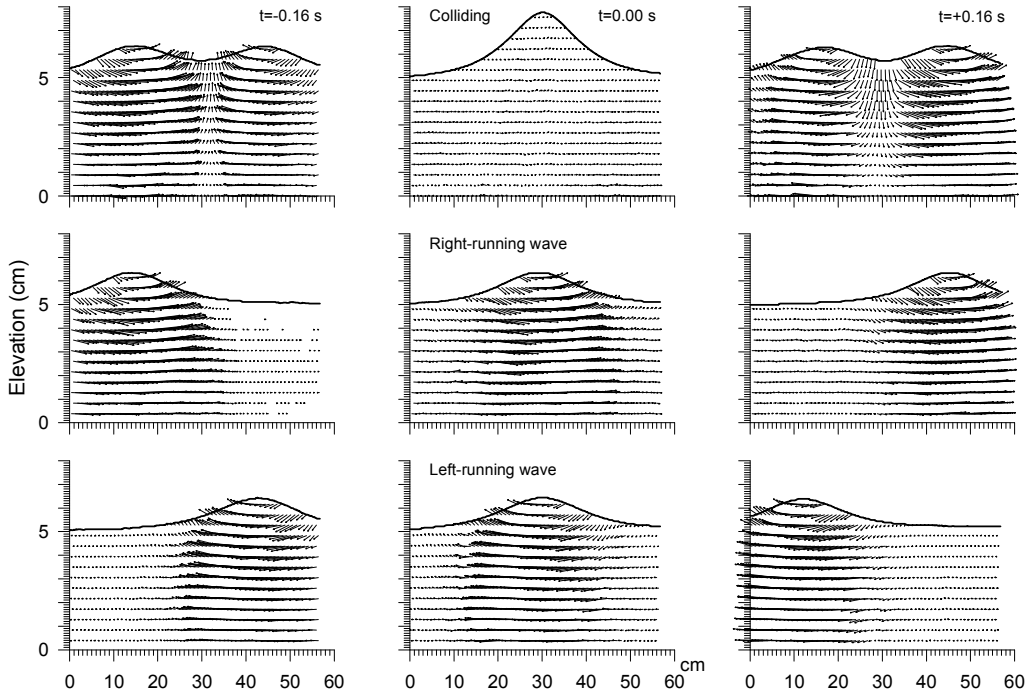


**Figure 9. Experimental results of velocity field for head-on collision (d=5 cm).**

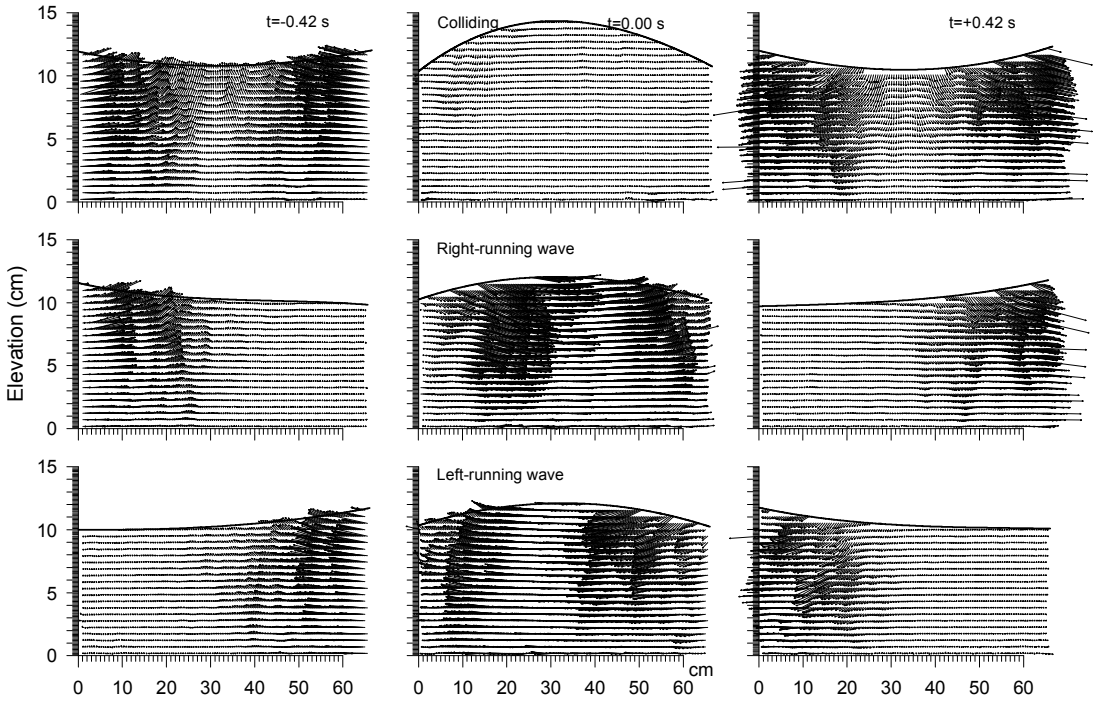


**Figure 10. Experimemtal results of velocity field for head-on collision (d=10 cm).**

The right-running wave is generated by a wave paddle motion and subsequently travels through a water body from one end to the other end of the tank, transporting energy as it moves. The wave propagates itself as the water particles interact; one particle applies a push or pull on its adjacent neighbor, causing a particle displacement from the rest position. A solitary wave has a distinct flow pattern that continues to move in an uninterrupted fashion until it encounters a boundary. When the right-running wave arrives at the end of the tank, it reflects and travels back in the opposite direction. This interference produces the left-running wave that has a new flow field, as shown in Figure 9(c), and indicates a contrasting pattern from the right-running wave in Figure 9(b). Flow patterns of the right-running (incident) and left-running (reflected) waves continue along the flume. When they meet up with one another in the test section, water particles produce a rather irregular and non-repeating flow pattern, as shown in Figure 9(a), which tends to change appearance over time. This irregular pattern is the result of the interference of an incident wave motion with a reflected wave motion in a rather non-sequenced manner. For example, at t=−0.16 s the water particles experience upwelling just ahead of each crest to generate a new crest of the colliding wave; at t=0.00 s they come to rest in an instant; and at t=0.16 s the water particles change direction downward in the space between both crests. Each flow pattern of the colliding wave is expected to be close to that of the superposition of the vectors given by right- and left-running waves. Later, uninterrupted traveling waves are observed in the flume. Another PIV result is a series of instantaneous velocity maps for WW2-2, as presented in Figure 10. Upon approaching the test section, the right- and left-running waves start their interference at t=−0.42 s. The right-running wave meets up with the left-running wave at t=0.00 s. As these two waves pass through each other, they undergo inversion until t=0.42 s. The figure shows snapshots of the interaction of the two waves at three different stages. The individual waves are shown in the middle and lower rows, and the resulting flow field is shown in the upper row. Careful inspection of the single and multiple wave velocity maps shows that the quasi-linear superposition principle is satisfied at all moments.

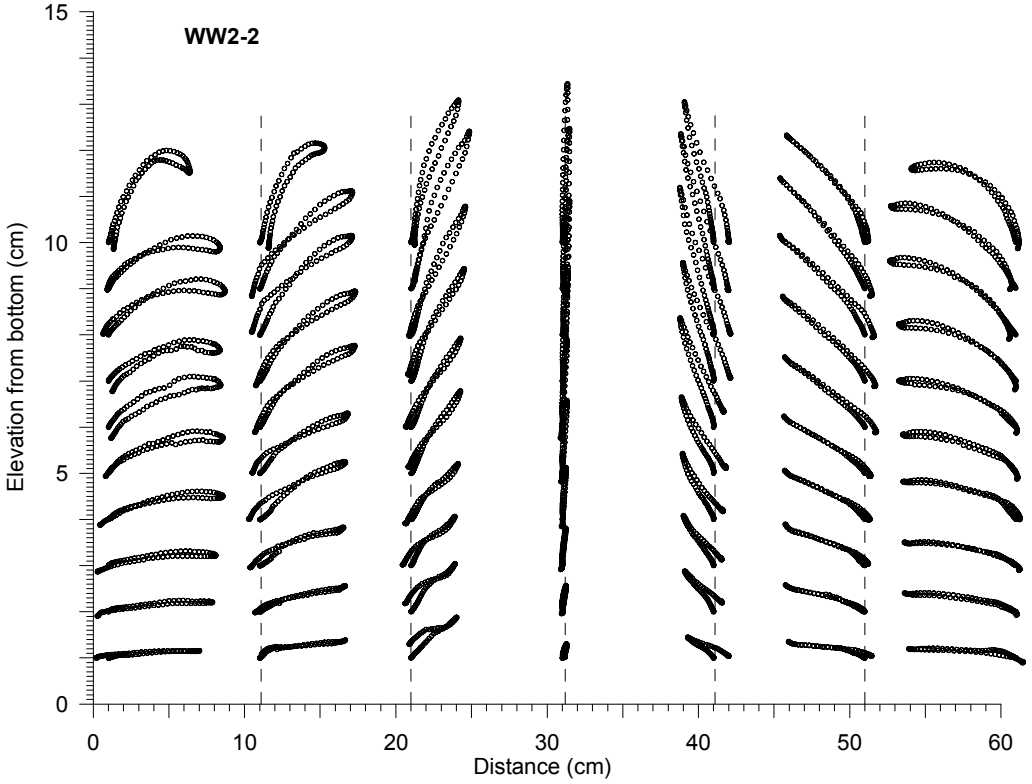


**Figure 11. Particle trajectories of head-on collision of two solitary waves (d=10 cm).**

Figure 11 shows the particle trajectories at seven cross sections for WW2-2. In each cross-section, we set the initial points at 1 cm intervals from the bottom to the surface. At the beginning, the water particle advances in the upper right or left direction to the first incident wave, and then moves a certain distance until the head-on collision occurs. It reaches a maximum level when the crests of the first and second solitary waves meet near the middle of the test section. After the collision, as the second wave approaches, the particle tends to return to its initial point. Most particles go back the way they came, but some do not turn back to the starting point. This asymmetric profile may be attributed to the difference between the two wave amplitudes, which attenuate due to dissipation during propagation and after the head-on collision.

## CONCLUSIONS

We experimentally investigated the spatial velocity variations for two different kinds of dual solitary wave collisions using PIV. In rear-end collisions, we generate a smaller wave first, and then generate a taller wave, which catches up and interacts with the smaller one, and then moves away from it. In head-on collisions, the first wave is reflected at the end of the flume and propagates back toward the wavemaker, and a second wave is generated so that these two waves meet at a prefixed location. We used the image thresholding method to capture various water-surface displacements. The observed data shows that the compound wave amplitude becomes smaller than the taller wave amplitude during rear-end collisions, but the colliding-wave amplitude is more than twice as large as the single-wave amplitude during head-on collisions. The experimental wave profiles suggest that there is a phase difference in each solitary wave before and after a head-on collision. We have not made a detailed inspection of the phase shift phenomenon because the horizontal distance of the test section was limited for some depth conditions. We presented instantaneous velocity vector maps to compare them with two single solitary wave results. We used a PIV algorithm to track water particle displacements. The high accuracy of the proposed approach could be applied to a Lagrangian description of the trajectory of a water particle for both rear-end and head-on collisions.

## REFERENCES

Airy, G.B. 1841. On tides and waves, *Encyclopedia Metro.*, London, 241-396.

Boussinesq, M.J. 1871. Théorie des ondes et des remous qui se propagent le long d'un canal réctangulaire horizontal, en communiquant au liquide contenu dans ce canal des vitesses sensiblement pareilles de la surface au fond, *J. Math. Pures Appl.*, 17, 55–108.

Byatt-Smith, J.G.B. 1971. An integral equation for unsteady surface waves and a comment on the Boussinesq equation, *J. Fluid Mech.*, 49, 625–633.

Byatt-Smith, J.G.B. 1987a. On the change of amplitude of interacting solitary waves, *J. Fluid Mech.*, 182, 485–497.

Byatt-Smith, J.G.B. 1987b. Perturbation theory for approximately integrable partial differential equations, and the change of amplitude of solitary-wave solutions of the BBM equation, *J. Fluid Mech.*, 182, 467–483.

Cauchy, A-L. 1827. Memoire sur la theorie de la propagation des ondes a la surface d'un fluide pesant d'une profondeur indefinie, Mem. Presentes Divers Savans Acad. R. Sci. Inst. France (Prix Acad. R. Sci., concours de 1815 et de 1816) I:3–312.

Chan, R.K.C. and R.L. Street. 1970. A computer study of finite-amplitude water waves, *J. Comput. Phys.*, 6, 68–94.

Constantin, A. 2011. Nonlinear water waves with applications to wave-current interactions and tsunamis, CBMS-NSF Regional Conference Series in Applied Mathematics, 81, 317p.

Coudraye, F.C. de Loynes. 1796. Theories des Vents et des Ondes, Copenhagen: Christensen. Kon. Ges. Wiss. Kopenhagen, 105–50.

Craig, W., P. Guyenne, J. Hammack., D. Henderson and C. Sulem. 2006. Solitary water wave interactions, *Phys. Fluids*, 18, 057106.

Dauxois, T. and M. Peyrard. 2006. Physics of Solitons, Cambridge, 422p.

Dean, R.G. and R.A. Dalrymple. 1984. Water Wave Mechanics for Engineers and Scientists, Prentice-Hall, Englewood Cliffs, NJ, 353p.

Drazin, P.G. and R.S. Johnson. 1989. Solitons: an Introduction, Cambridge, 226p.

Fenton, J.D. 1972. A ninth–order solution for the solitary wave, *J. Fluid Mech.*, 53, 257–271.

Fenton, J.D. and M. Rienecker. 1982. Fourier method for solving nonlinear water-wave problems: application to solitary-wave interactions, *J. Fluid Mech.*, 118, 411–443.

Fermi, E., J. Pasta, and S.M. Ulam. 1955. Studies in nonlinear problems, *Tech. Rep.*, LA-1940, Los Alamos Sci. Lab.

Flaugergues, M. 1793. Hollandsche Maatschappye der Weetenschappen te Haarlem, xxix Deel, p. 131.

Gerstner, F.J. von. 1802. Theorie der Wellen. Abhand. Kon. Bohmischen Gesel. Wiss., Prague.

Goring, D.G. 1979. Tsunamis –The propagation of long waves onto a shelf, Ph.D. thesis, Caltech, 337p.

Green G. 1838. On the motion of waves in a variable canal of small depth and width, *Trans.* Camb. Philos. Soc. 6:457–462.

Hammack, J., D. Henderson, P. Guyenne and Y. Ming. 2004. Solitary–wave collisions, A Symp. to honor Theodore Yao–Tsu Wu, *OMAE 2004*, ASME, 1–12.

Hirota, R. 1971. Exact solution of Korteweg-de Vries equation for multiple collisions of solitons, *Phys. Rev. Lett.*, 27, 1192-4.

Kelland, P. 1840. On the theory of waves, Part 1. *Trans. Roy. Soc. Edinburgh*, 14:497–545.

Korteweg, D.J. and G. deVries. 1895. On the change of form of long waves advancing in a rectangular canal and on a new type of long stationary waves, *Phil. Mag.*, 39, 422–443.

Laitone, E.V. 1960, The Second Approximation to Cnoidal and Solitary Waves, *J. Fluid Mech.*, 9, 430–444.

Marchant, T.R and N.F. Smyth. 1990. The extended Korteweg-de Vries equation and the resonant flow of a fluid over topography, *J. Fluid Mech.*, 221, 263–288.

Maxworthy, T. 1976. Experiments on collisions between solitary waves, *J. Fluid Mech.*, 76, 177–185.

Mirie, R.M. and C.H. Su. 1982. Collisions between two solitary waves. Part 2. A numerical study, *J. Fluid Mech.*, 115, 475-492.

Poisson, S.D. 1818. Memoire sur la theorie des ondes, *Mem.* Acad. R. Sci. Inst. France. 1816, 2nd Ser. 1:70–186.

Rayleigh, Lord. 1876. On waves, *Phil. Mag.* (5), 1, 257-279.

Remoissenet, M. 1999. Waves Called Solitons: Concepts and Experiments, Springer, 327p.

Renouard, D., F. Santos and A. Temperville. 1985. Experimental study of the generation, damping, and reflexion of a solitary wave, *Dyn. Atmos. Oceans*, 9, 341–358.

Russell, J.S. 1844. Report on waves, *Rep. Meet. Brit. Assoc. Adv. Sci.*, 14, 311–390.

Russell, J.S. and J. Robison. 1837. Report on waves, *Rep.*, Br. Assoc. Adv. Sci., 417–496.

Schwartz, L.W. 1974. Computer extension and analytic continuation of Stokes' expansion for gravity waves, *J. Fluid Mech.*, 62, 553–578.

Shimizu, R., T. Shintani and M. Umeyama. 2006. Instantaneous and Lagragian velocity fields of internal waves on a slope by PIV measurement and numerical simulation, *Annu. J. Coast. Eng.*, JSCE, 52, 1-5.

Stokes, G.G. 1847. On the theory of oscillatory waves, *Trans. Cambridge Phil. Soc.*, 8 (441).

Su, C.H. and R.M. Mirie. 1980. On head-on collisions between two solitary wave, *J. Fluid Mech.*, 98, 509-525.

Umeyama, M. 2008. PIV techniques for velocity fields of internal waves over a slowly varying bottom topography, *J. Water., Port, Coast. & Oc. Eng.*, ASCE, 134(5), 286-298.

Umeyama, M. 2011. Coupled PIV and PTV measurements of particle velocities and trajectories for surface waves following a steady current, *J. Water., Port, Coast. & Oc. Eng.*, ASCE, 137(2), 85-94.

Umeyama, M. 2012. Eulerian/Lagrangian analysis for particle velocities and trajectories in a pure wave motion using particle image velocimetry, In a Theme Issue 'Nonlinear Water Waves' edited by Adrian Constantin, *Phil. Trans. Roy. Soc. A*, Roy. Soc. Pub., 370(1964), 1687-1702.

Umeyama, M. 2013. Investigation of single and multiple solitary waves using superresolution PIV, J. *Water., Port, Coast. & Oc. Eng.*, ASCE, 139(4), 303-313.

Umeyama, M. and S. Matsuki. 2011. Measurements of velocity and trajectory of water particle for internal waves in two density layers, *Geo. Res. Lett.*, AGU, 38, L03612.

Umeyama, M. and K.-C. Nguyen. 2012. PIV measurements of particle velocities and trajectories for internal waves propagating in a two-layer fluid on a sloping boundary, *Proc., ICCE*, ASCE, 33, currents.54.

Umeyama, M. and H. Shinomiya. 2009. Particle image velocimetry measurements for Stokes progressive internal waves, *Geo. Res. Lett.*, 36(6), AGU, L06603.

Umeyama, M., T. Shintani and S. Watanabe. 2010. Measurements of particle velocities and trajectories in a wave-current motion using PIV and PTV, *Proc., ICCE*, ASCE, 32, Waves.2.

Umeyama, M., T. Shintani, K.-C. Nguyen and S. Matsuki. 2012. Measurements of particle velocities and trajectories for internal waves propagating in a density-stratified two-layer fluid on a slope, Chapter 12 in "Particle Image Velocimetry" edited by Cavazzini Giovanna, InTech, 321-344.

Weber, E.H. and W.E. Weber. 1825. Wellenlehre auf Experimente gegrundet, Leipzig: Gerhardt Fleischer.

Weidman, P. and T. Maxworthy. 1978. Experiments on strong interactions between solitary waves, *J. Fluid Mech.*, 85, 417–431.

Zabusky, N.J. and M.D. Kruskal. 1965. Interaction of solitons in a collisionless plasma and the recurrence of initial states, *Phys. Rev. Lett.*, 15, 240-3.